

A novel X-ray tube spectra reconstruction method based on transmission measurements

Jing Cao^{1,2} · Chun-Yu Jiang^{1,2} · Yan-Feng Zhao^{1,2} · Qing-Wei Yang³ · Ze-Jie Yin^{1,2}

Received: 23 December 2014/Revised: 30 August 2015/Accepted: 31 August 2015/Published online: 12 April 2016
© Shanghai Institute of Applied Physics, Chinese Academy of Sciences, Chinese Nuclear Society, Science Press China and Springer Science+Business Media Singapore 2016

Abstract A novel X-ray tube spectrum reconstruction method has been proposed based on transmission measurements. Aluminum bars of varying lengths attenuate the X-rays to different levels. The detectors are of lutetium yttrium oxyorthosilicate scintillator and silicon photomultiplier. With the detected X-ray intensities, the X-ray spectrum is unfolded using the least square method. The detectors, aluminum bars, and collimating apertures are integrated in a detection module made of lead. Its response to X-ray is calculated by Monte Carlo codes Geant4. Due to the high photon flux, the detectors work in current mode. The electronics system, consisting of 24-bit high-precision ADCs with 144KSPS sampling rate and field programmable gate array, makes the data acquisition process effective and precise. Measurements on a 70-kVp tungsten anode X-ray were taken to verify the method. The unfolded spectrum agrees well with the simulated spectrum, demonstrating that the method is reliable and practical.

Keywords X-ray tube · Spectrum unfolding · Transmission measurements · Geant4 · LYSO · SiPM

Supported by National Natural Science Foundation of China (Nos. 11375195, 11375263) and National Magnetic Confinement Fusion Science Program of China (2013GB104003).

✉ Jing Cao
jcao@mail.ustc.edu.cn

¹ State Key Laboratory of Particle Detection and Electronics, University of Science and Technology of China, Hefei 230026, China

² Department of Modern Physics, University of Science and Technology of China, Hefei 230026, China

³ Southwestern Institute of Physics, Chengdu 610041, China

1 Introduction

X-ray tubes are widely used in scientific research, medical diagnostics, engineering inspection, etc., such as X-ray fluorescence (XRF) [1, 2], computed tomography [3], and X-ray nondestructive test [4]. X-ray spectrum is quite important to precise dosimetry estimation and improves the image quality in radiodiagnostic applications. Due to the high intensity and dose rate, it is difficult to measure an X-ray spectrum directly. The high fluence rate of photons would make scintillation or semiconductor detectors face serious problems of signal distortion and pile-up, so the traditional method of pulse-height analysis [5] is no longer applicative.

Transmission measurements [6–8], Monte Carlo (MC) simulation [9, 10], and theoretical calculation based on empirical or semiempirical physical models [11–13] have become common methods for X-ray spectrum determination. The results from MC simulation and theoretical calculation are affected by precision of the simplified model of the X-ray tube and related structures such as the collimator, because the geometric structure and the related particle transport in a particular X-ray machine are complex, and some degree of inaccuracy is unavoidable. Thus, the simulation or calculation results need to be verified by measurements. Transmission measurements were first proposed by Silberstein [14] and developed by many researchers [15–18]. In our previous work, this method was used to measure the bremsstrahlung spectrum generated by a 20-MV linear induction accelerator with iron attenuation and alanine dosimeter [19]. The X-ray spectra were reconstructed from attenuation measurement data. It was quite easy to operate and suitable for a wide range of photon energy, though the energy resolution was not so good.

Fig. 1 Structure sketch (a) and picture (b) of the integrated detection module. 1 incident X-rays; 2 Pb collimator; 3 $\phi 2 \text{ mm} \times 7 \text{ cm}$ collimating aperture; 4 Al bars; 5 LYSO scintillator, sized as $3 \text{ mm} \times 3 \text{ mm} \times 11 \text{ mm}$, and covered with 0.05-mm-thick aluminum foil; 6 SiPM; 7 the backside hole of $\phi 6.3 \text{ mm} \times 3 \text{ cm}$ to insert the detector, a heat-shrinkable tube package of LYSO and SiPM

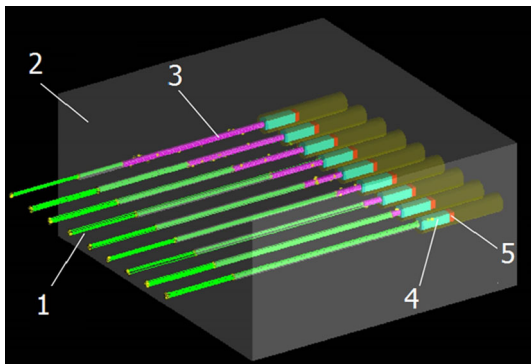
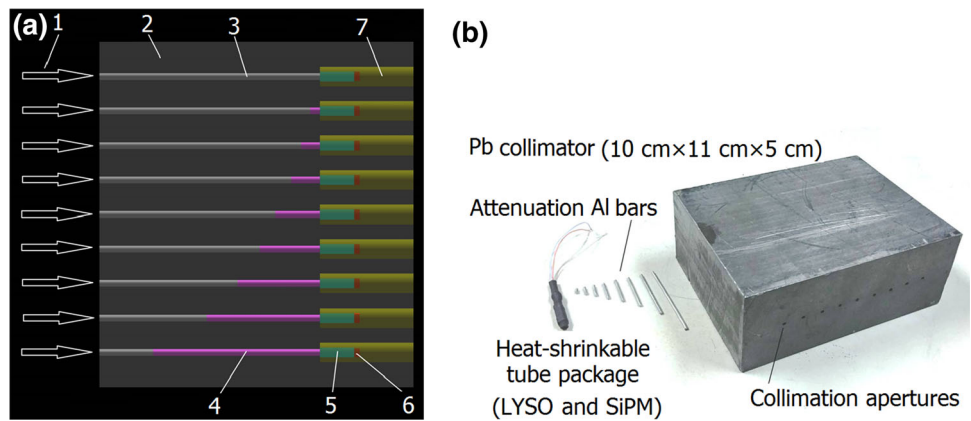


Fig. 2 The simulation environment in Geant4. 1 trajectories of incident X-rays in each collimating apertures; 2 collimator of pure lead; 3 bars of pure aluminum; 4 LYSO scintillator, $\text{Lu}_{0.6}\text{Y}_{1.397}\text{-Ce}_{0.003}(\text{SiO}_4)\text{O}$, covered with 0.05 mm Al foil; 5 SiPM, set as air

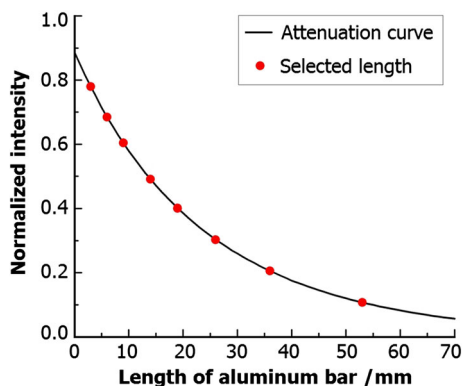


Fig. 3 The attenuation curve of the aluminum bars in this detection module and the eight selected length

In this paper, a novel X-ray spectrum reconstruction method based on transmission measurements is presented. In Sect. 2, the basic mathematics is described. In Sect. 3, the novel method is introduced in detail, including its integrated detection module, the detectors composed of lutetium yttrium

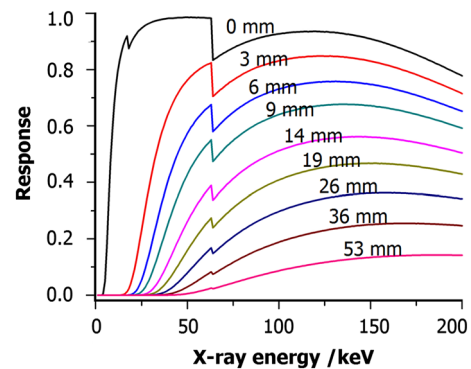


Fig. 4 Calculated response to X-ray of the integrated detection module with aluminum bars of different lengths

oxyorthosilicate scintillator (LYSO) [20] and silicon photomultiplier (SiPM) [21], the design based on MC simulation [22, 23], and response of the detection module to X-rays. In Sect. 4, the associated data acquisition electronic system was presented. Meanwhile, X-ray spectrum of a 70-kVp tungsten anode X-ray tube agrees well with simulated spectrum, indicating that the method is reliable and practical.

2 Mathematical principle

Attenuation of X-ray in material is energy-dependent, so intensity of the transmitted X-rays contains information of energy distribution of the X-rays. There is a mathematic possibility to unfold the X-ray spectrum. It is the principle of transmission measurements, which can be described by the Fredholm integral equation as follows. X-rays with a certain energy distribution irradiating several pure materials of different thickness are attenuated differently, and intensity of the transmitted X-rays can be detected as:

$$N_i = \int D(E)\phi(E)e^{(-\mu(E)h_i)}dE, \quad i = 1, 2, \dots, m, \quad (1)$$

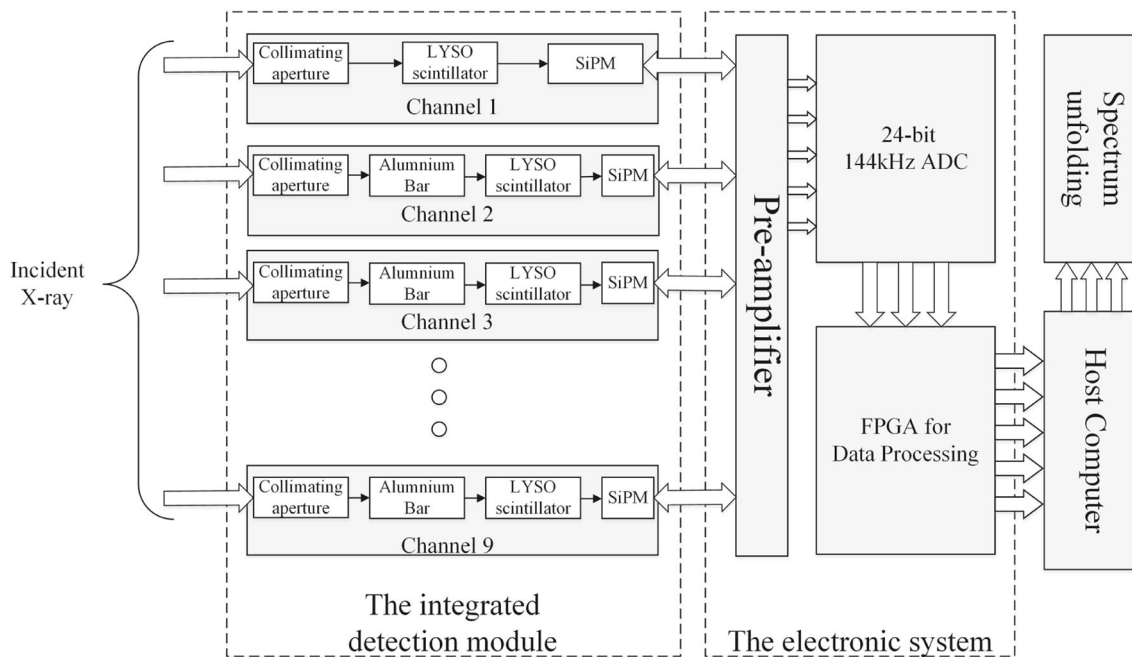


Fig. 5 The block diagram of the X-ray spectrum measurement system

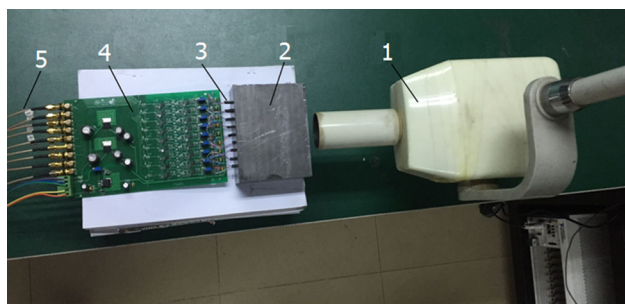


Fig. 6 The spectrum measurement of an X-ray apparatus. 1 70-kVp tungsten anode X-ray tube; 2 collimator; 3 detectors inserted in backside holes of the collimator; 4 preamplifier; 5 wires for output signals

where $\Phi(E)$ is the intensity spectrum of the incident X-rays; $\mu(E)$ is the linear attenuation coefficient of X-rays in the pure attenuation material; h_i is thickness of the i th attenuation material; $D(E)$ is detection efficiency of the detectors; N_i is transmitted X-ray intensity measured by the detectors. After discretization, Eq. (1) become

$$N_i = \sum_{j=1}^n R_{ij}\phi_j, \quad i = 1, 2, \dots, m, \quad (2)$$

where R combines the $D(E)$ and $e^{(-\mu(E)h_i)}$ part in Eq. (1) for convenience and is called the response matrix. The problem is ill-posed, since the number of attenuation materials is quite limited, far less than the discrete points ($m < n$), the problem cannot be solved directly. In this work, the least square method [24] was used to unfold the discretized X-ray spectrum in Eq. (2), since it is quite simple and efficient.

3 Methods

All the attenuation materials and the detectors are installed in an integrated detection module (Fig. 1). The X-ray detector is LYSO plus SiPM packaged in a heat-shrinkable tube (Fig. 1b), which is inserted in the backside placement hole. Aluminum bars of different length are inserted in the collimating apertures in front of the backside holes. The incident X-rays are collimated by the nine collimating apertures. This detection module is made of lead, so X-rays in different channels shall not affect one another. The aluminum bars attenuate the X-rays to different degrees (there is no aluminum bar in the channel no. 1). The LYSO scintillators absorb the attenuated X-rays and convert them into plenty of visible photons. The backside SiPMs detect the visible photons and generate electronic signals which are amplified and acquired by the electronic system. The X-ray intensities of the nine channels are used for the spectrum unfolding.

The module was designed on basis of MC simulation using Geant4.10.01. The standard electromagnetic process library of G4EmStandardPhysics_option3 was chosen, since it is the best for medical and space applications. In the energy range of below 200 keV, the dominate physics process of X-rays in matter is photoelectric effect and Compton scattering. The simulation geometric structure is based on the real structure of the detection module as illustrated in Fig. 2. The SiPM part is set as air since it is unused in simulation. We just gather the energy deposition in LYSO, which is almost proportional to the sum of generated visible photons and the strength of the output

Fig. 7 A typical output signal of the detector working in current mode on this experiment

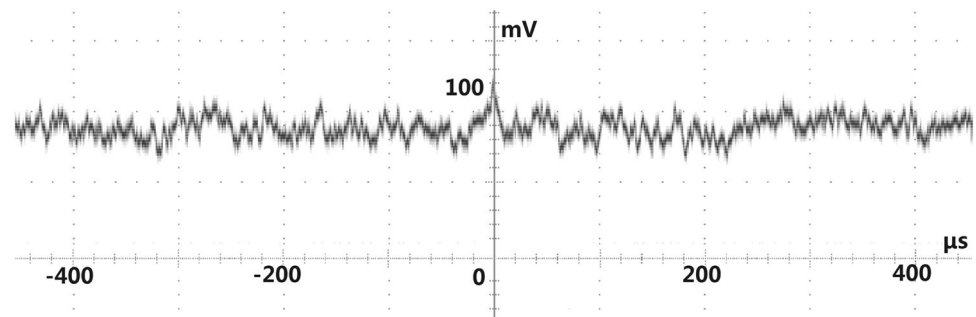


Table 1 The measured X-ray intensities corresponding to the nine channels

Channels	1	2	3	4	5	6	7	8	9
Aluminum bar length (mm)	0	3	6	9	14	19	26	36	53
X-ray intensity (normalized)	1.0000	0.5920	0.3800	0.2270	0.1273	0.0606	0.0323	0.0101	0.0029

signal of the SiPMs; the complex and time-consuming track of plenty of scintillate photons is unnecessary.

Firstly, the best lengths for the eight aluminum bars were determined via the MC simulation, in which the aluminum bar increased from 1 to 70 in 1 mm steps, and X-rays of certain intensity were collimated to travel through each of the Al bars. Energy of the incident X-ray is random below 200 keV without loss of generality; energy deposition in LYSO is normalized to the incident X-ray intensity. The attenuation curve acquired is shown in Fig. 3. Based on the attenuation curve, the selected lengths of Al bar are 3, 6, 9, 14, 19, 26, 36, and 53 mm.

The response matrix in Eq. (2) is important for the X-ray spectrum unfolding. Theoretical calculation is complex and unsuitable to specific structure of the detection module. In this work, it was obtained through Geant4 simulation, with the eight aluminum bars selected in Fig. 3. Monoenergetic photons were used, with the energy varied from 1 to 200 keV in 1-keV steps. For each energy point, 10^8 photons were simulated and the energy deposition in each LYSO was gathered. In this way, the response matrix of all detectors to X-rays can be calculated as shown in Fig. 4. Some leaps in these curves can be observed; one is in the 0-mm curve at 18 keV, which is closed to the K edge of yttrium ($K\alpha$ X-ray of 17.037 keV), and the exited characteristic X-rays are most likely to escape from the detector's side, causing the decrease in detection efficiency. Other leaps are at 64 keV, which is closed to the K edge of lutetium ($K\alpha$ X-ray of 63.304 keV), hence the decrease in detection efficiency. Above certain energy of for each length of the aluminum bars, e.g., about 150 keV for 26 mm, the response decreased slightly, as an LYSO of limited length cannot absorb completely the X-rays of higher energies.

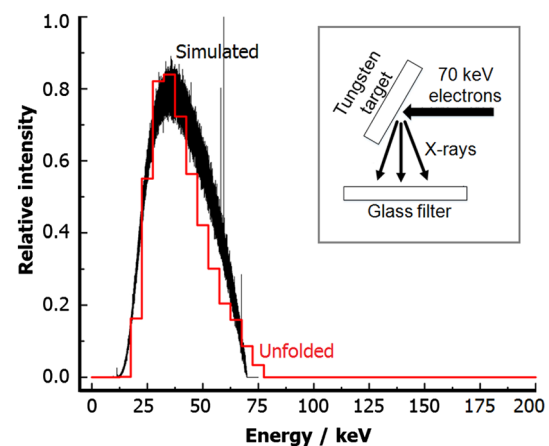


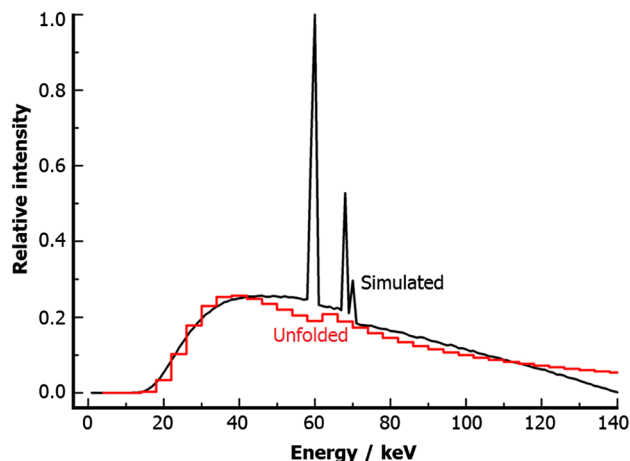
Fig. 8 The unfolded and simulated X-ray spectra. The *insert* shows the geometry of simulating the 70-keV electrons

4 Experiment validation

The SiPMs were purchased from SensL Ltd. of Ireland (B-series, type: MicroFB-30035-SMT), and LYSO crystals were manufactured by Shanghai Institute of Ceramics, Chinese Academy of Sciences. For the high photon flux from X-ray tubes, the detectors work in current mode, which should be DC coupled. The current passes through a certain resistance and outputs a steady voltage; the X-ray intensity is detected by measuring the output voltage. The data acquisition system is illustrated in Fig. 5). The output voltages were amplified by a preamplifier to satisfy the input requirements of the ADCs. The high-precision ADCs (type: ADS1278, TI Ltd., USA) with a 24-bit resolution, and upmost 144 KSPS sampling rate is used to digitize the steady voltage and the produced digital data streams are transferred to the field programmable gate array (FPGA) for data processing. All the sampled digitized data during

Table 2 The LYSO energy deposition corresponding to the nine channels in Geant4 simulation

Channel	1	2	3	4	5	6	7	8	9
Aluminum bar length (mm)	0	3	6	9	14	19	26	36	53
E_{dep} (normalized)	1.0000	0.7604	0.5950	0.4750	0.3355	0.2424	0.1578	0.0884	0.0351

**Fig. 9** The unfolded spectrum of 140-kVp tungsten anode X-ray tube from simulation data in comparison with simulated spectrum

the X-ray tube reaction period are averaged in the FPGA (Cyclone III series, Altera Ltd., USA) and then uploaded to the host computer. The output voltages corresponding to the nine channels are used for spectrum unfolding.

This method was used to measure the photon spectrum of an X-ray apparatus (type: LXY-7002, Dandong Aolong Radiative Instrument Co., Ltd, China) as shown in Fig. 6. The X-ray apparatus contains a micro-focus (0.3×0.3 mm) tungsten anode X-ray tube of 2 mA current. Due to its limited intensity, the X-ray scanner is quite suitable to the detection module. Each of the nine collimating apertures is irradiated by X-rays from a certain distance. Figure 7 is a typical output signal of the detectors. A nine-channel preamplifier amplifies the signals and transports them through SMA cables. The normalized X-ray intensities corresponding to the nine channels are given in Table 1.

To unfold the photon spectrum, 40 points were selected from the response matrix in Fig. 4 from 5 to 200 keV in 5-keV steps. According to Eq. (2), the photon spectrum was finally unfolded based on the selected response matrix, the measured X-ray intensity (Table 1) and the least square method [12], as shown in Fig. 8.

To validate the unfolded spectrum, a Geant4 simulation of the 70-kVp tungsten anode X-ray tube was done to acquire its photon spectrum. With low-energy (70 keV) electrons, the physics process in Geant4 was switched to G4EmLowEPPysics. The simulation geometry is shown in

the insert of Fig. 8. Electrons of 70 keV were set to strike the tungsten target of 2 mm thickness, and the X-rays were filtered by a glass window. The transmitted photons were gathered, and the X-ray energy spectrum was acquired. The simulated spectrum using 5.4×10^{10} electrons is shown in Fig. 8, in comparison with the unfolded spectrum. Although some degree of statistical fluctuation remains, due to the limited computing capability for this time-consuming Geant4 simulation, it can be seen that the defolded and simulated spectra agree well to each other.

To further validate this method, a simulation about spectrum measurement on X-ray tube generating 140-keV electron beams. The initial number of electrons was 1×10^9 . The energy depositions gathered in the nine LYSOs are given in Table 2 (it is proportional to the measured X-ray intensity and can be used for spectrum unfolding). In this way, we simulated the spectrum measurement process of 140-keV electrons. The X-ray spectrum was unfolded with the data in Table 2 and the response function in Fig. 4. Figure 9 shows the simulated and unfolded spectra.

The two spectra are of remarkable consistency, but they differ apparently above 110 keV. The reason is that all the response curves become quite flat above 110 keV. Because of the small difference of response, the spectral information cannot be acquired through the same response to all energy components in this energy range, since the principle of transmission measurements is to associate the transmission data to the spectral distribution. If the energy response is the same, the association does not exist. Therefore, to some degree, this method may take the risk of inaccuracy for an X-ray tube of over 110 kVp.

5 Conclusion

A novel method for X-ray tube spectrum reconstruction has been presented based on transmission measurements, with an integrated detection module. The detectors are LYSO and SiPM, working in current mode. The 144 KSPS sampling rate of the high-precision 24-bit ADC and the data processing ability of FPGA make the data acquisition process effective and precise. The detectors, attenuation aluminum bars, and collimating apertures are integrated in a detection module made of lead. The response to X-ray

was simulated by Geant4. The spectrum measurement of a 70-kVp X-ray tube was carried out and the unfolded spectrum was quite close to the simulated spectrum, indicating that this method is reliable and practical. A simulation measurement on 140-kVp X-ray tube revealed its weakness in energy range above 110 keV, since the response functions above 110 keV are quite flat; the spectral information is missing by transmission analysis. So this method is only applicative for X-ray tube below 110 kVp.

The characteristic X-rays of 58.117, 59.484, and 67.418 keV can be seen in the simulated X-ray spectra in Figs. 8 and 9, but they are missing in the unfolded spectrum, because resolution of the transmission measurements is quite low and the discrete energy points selected for the unfolding procedure are quite limited in Eq. (2). The resolution can be improved by collecting more transmission data or using better unfolding algorithm.

In future work, this method will be applied to X-ray tubes of higher voltages, with different anode material and filters. Structure of the integrated detection module shall be improved, such as its best dimension and channel number.

References

1. J. Wang, M.Z. Liu, X.G. Tuo et al., A genetic-algorithm-based neural network approach for EDXRF analysis. *Nucl. Sci. Tech.* **25**, 030203 (2014). doi:[10.13538/j.1001-8042/nst.25.030203](https://doi.org/10.13538/j.1001-8042/nst.25.030203)
2. T. Tian, J.C. Zhang, H.Z. Lei et al., Synchrotron radiation X-ray fluorescence analysis of Fe, Zn and Cu in mice brain associated with Parkinson's disease. *Nucl. Sci. Tech.* **26**, 030506 (2015). doi:[10.13538/j.1001-8042/nst.26.030506](https://doi.org/10.13538/j.1001-8042/nst.26.030506)
3. M. Chang, Y.S. Xiao, Z.Q. Chen, An industrial CT system for monitoring a running aero-engine. *Nucl. Sci. Tech.* **25**, 060202 (2014). doi:[10.13538/j.1001-8042/nst.25.060202](https://doi.org/10.13538/j.1001-8042/nst.25.060202)
4. M.C. Chen, L.H. Tian, Mass thickness measurements for dual-component samples utilizing equivalent energy of X-rays. *Nucl. Sci. Tech.* **25**, 040202 (2014). doi:[10.13538/j.1001-8042/nst.25.040202](https://doi.org/10.13538/j.1001-8042/nst.25.040202)
5. G.Q. Zeng, C.J. Tan, Q. Luo et al., A nuclear spectrum generator for semiconductor X-ray detectors. *Nucl. Sci. Tech.* **25**, 030403 (2014). doi:[10.13538/j.1001-8042/nst.25.030403](https://doi.org/10.13538/j.1001-8042/nst.25.030403)
6. V. Delgado, Determination of X-ray spectra from Al attenuation data by imposing a prior physical features of the spectrum: theory and experimental validation. *Med. Phys.* **36**, 142–148 (2009). doi:[10.1118/1.3031117](https://doi.org/10.1118/1.3031117)
7. X.H. Duan, J. Wang, L.F. Yu et al., CT scanner X-ray spectrum estimation from transmission measurements. *Med. Phys.* **38**, 993–997 (2011). doi:[10.1118/1.3547718](https://doi.org/10.1118/1.3547718)
8. M. Endrizzi, P. Delogu, P. Oliva, Application of an expectation maximization method to the reconstruction of X-ray-tube spectra from transmission data. *Spectrochim. Acta Part B* **102**, 42–47 (2014). doi:[10.1016/j.sab.2014.10.009](https://doi.org/10.1016/j.sab.2014.10.009)
9. I. Jerez-Sainz, A. Perez-Rozos, A.M. Lallena, Monte Carlo analysis of the degradation of the spectrum produced by an X-ray tube in conventional radiography. *Nucl. Instrum. Methods A* **580**, 518–521 (2007). doi:[10.1016/j.nima.2007.05.219](https://doi.org/10.1016/j.nima.2007.05.219)
10. R. Taleei, M. Shahriari, Monte Carlo simulation of X-ray spectra and evaluation of filter effect using MCNP4C and FLUKA code. *Appl. Radiat. Isot.* **67**, 266–271 (2009). doi:[10.1016/j.apradiso.2008.10.007](https://doi.org/10.1016/j.apradiso.2008.10.007)
11. G.G. Poludniowski, Calculation of X-ray spectra emerging from an X-ray tube. Part II. X-ray production and filtration in X-ray targets. *Med. Phys.* **34**, 2175–2186 (2007). doi:[10.1118/1.2734726](https://doi.org/10.1118/1.2734726)
12. M. Caon, G. Bibbo, J. Pattison et al., The effect on dose to computed tomography phantoms of varying the theoretical X-ray spectrum: a comparison of four diagnostic X-ray spectrum calculating codes. *Med. Phys.* **25**, 1021–1027 (1998). doi:[10.1118/1.598281](https://doi.org/10.1118/1.598281)
13. J.M. Boone, J.A. Seibert, An accurate method for computer-generating tungsten anode X-ray spectra from 30 to 140 kV. *Med. Phys.* **24**, 1661–1670 (1997). doi:[10.1118/1.597953](https://doi.org/10.1118/1.597953)
14. L. Silberstein, Determination of the spectral composition of X-ray radiation from filtration data. *J. Opt. Soc. Am.* **22**, 265–280 (1932). doi:[10.1364/JOSA.22.000265](https://doi.org/10.1364/JOSA.22.000265)
15. R.G. Waggener, M.M. Blough, J.A. Terry et al., X-ray spectra estimation using attenuation measurements from 25 kVp to 18 MV. *Med. Phys.* **26**, 1269–1278 (1999). doi:[10.1118/1.598622](https://doi.org/10.1118/1.598622)
16. J.R. Lei, S.Y. Ran, Y.G. Yuan et al., Reconstruction of 12 MV bremsstrahlung spectra from measured transmission data. *Nucl. Sci. Tech.* **14**, 138–143 (2003)
17. M. Manciu, F.S. Manciu, T. Vulcan et al., Robust megavoltage X-ray spectra estimation from transmission measurements. *J. Xray Sci. Technol.* **17**, 85–99 (2009). doi:[10.3233/XST-2009-0214](https://doi.org/10.3233/XST-2009-0214)
18. E.S.M. Ali, D.W.O. Rogers, An improved physics-based approach for unfolding megavoltage bremsstrahlung spectra using transmission analysis. *Med. Phys.* **39**, 1663–1675 (2012). doi:[10.1118/1.3687164](https://doi.org/10.1118/1.3687164)
19. J. Cao, R. Xiao, N. Chen et al., Spectral reconstruction of the flash X-ray generated by Dragon-I LIA based on transmission measurements. *Nucl. Sci. Tech.* **26**, 040403 (2015). doi:[10.13538/j.1001-8042/nst.26.040403](https://doi.org/10.13538/j.1001-8042/nst.26.040403)
20. C.M. Pepin, P. Berard, A.L. Perrot et al., Properties of LYSO and recent LSO scintillators for phoswich PET detectors. *IEEE Trans. Nucl. Sci.* **51**, 789–795 (2004). doi:[10.1109/TNS.2004.829781](https://doi.org/10.1109/TNS.2004.829781)
21. P. Buzhan, B. Dolgoshein, L. Filatov et al., Silicon photomultiplier and its possible applications. *Nucl. Instrum. Methods A* **504**, 48–52 (2003). doi:[10.1016/S0168-9002\(03\)00749-6](https://doi.org/10.1016/S0168-9002(03)00749-6)
22. S. Agostinelli, J. Allison, K. Amako et al., Geant4—a simulation toolkit. *Nucl. Instrum. Methods A* **506**, 250–303 (2003). doi:[10.1016/S0168-9002\(03\)01368-8](https://doi.org/10.1016/S0168-9002(03)01368-8)
23. O. Kadri, M.A. Alnafea, K. Shamma, Computation and parameterization of normalized glandular dose using Geant4. *Nucl. Sci. Tech.* **26**, 030303 (2015). doi:[10.13538/j.1001-8042/nst.26.030303](https://doi.org/10.13538/j.1001-8042/nst.26.030303)
24. S. Tominaga, The estimation of X-ray spectral distributions from attenuation data by means of iterative computation. *Nucl. Instrum. Methods A* **192**, 415–421 (1982). doi:[10.1016/0029-554X\(82\)90853-9](https://doi.org/10.1016/0029-554X(82)90853-9)